Enhancing relativistic electron beam propagation through the use of graded resistivity guides

R. A. B. Alraddadi, A. P. L. Robinson, J. Pasley, and N. C. Woolsey

Citation: Physics of Plasmas **25**, 023104 (2018); doi: 10.1063/1.5004265
View online: https://doi.org/10.1063/1.5004265
View Table of Contents: http://aip.scitation.org/toc/php/25/2
Published by the American Institute of Physics

Enhancing relativistic electron beam propagation through the use of graded resistivity guides

R. A. B. Alraddadi,[1,a)] A. P. L. Robinson,[2] J. Pasley,[3,2] and N. C. Woolsey[3]
[1]*Department of Physics and Astronomy, College of Science, King Saud University, P. O. Box 2455 Riyadh 11451, Saudi Arabia*
[2]*Central Laser Facility, STFC Rutherford-Appleton Laboratory, Didcot OX11 0QX, United Kingdom*
[3]*York Plasma Institute, Department of Physics, University of York, York YO10 5DD, United Kingdom*

(Received 12 September 2017; accepted 30 January 2018; published online 13 February 2018)

We show, using three dimensional hybrid particle-in-cell simulations, that fast electron transport is improved in a resistive guide when using a linear decreasing gradient in the resistivity between the guide and substrate. We observe increased heating-at-depth along the guide and significantly reduced heating inhomogeneity. These improvements result from an increase in the width of the collimating magnetic field, improving fast electron confinement and limiting the growth of magnetic fields in the interior of the guide. *Published by AIP Publishing.* https://doi.org/10.1063/1.5004265

I. INTRODUCTION

The interaction of an ultra-intense laser ($I_L\lambda_L > 10^{18}$ W cm$^{-2}\mu$m^2) with a solid target results in multi-mega-Ampere currents of fast electrons and the formation of hot solid density plasma.[1] These fast electrons are highly divergent[2,3] with their transport affected by self-generated magnetic fields.[4,5] These magnetic fields can result in self-pinching, resistive collimation[6] and filamentation[7] of the fast electron beam. The growth rate of the magnetic field is described by the induction equation as[5]

$$\frac{\partial \vec{B}}{\partial t} = \eta(\nabla \times \vec{j_f}) + (\nabla\eta) \times \vec{j_f}, \tag{1}$$

where $\vec{B}$ is the flux density of the magnetic field, η is the resistivity, and $\vec{j_f}$ is the fast electron current density. Equation (1) indicates two principal ways to generate a magnetic field are through a spatial variation in (a) the fast electron current density and/or (b) the target resistivity. The resistive guiding concept, introduced by Robinson and Sherlock,[8] exploits Eq. (1) to generate an azimuthal magnetic field that confines electrons to regions of high resistivity enclosed by regions of low resistivity. Resistive guides can be in the form of a wire,[9] strip[10] or conical[11,12] shaped targets with a high atomic number (and high resistivity) core embedded in a lower atomic number substrate. The resistivity gradient is created by placing two or more materials next to each other and is typically engineered in the direction transverse to the axis of the fast electron beam. The collimation of the fast electrons in the resistive guide occurs as follows: in the early stages of the laser–target interaction, the $(\nabla\eta) \times \vec{j_f}$ term produces a strong azimuthal magnetic field which pushes the fast electrons into regions of higher resistivity, the core of the resistive guide. The resulting collimation causes a gradient in the fast electron current density, so the $\eta(\nabla \times \vec{j_f})$ further increases the magnetic field and enhances the collimation.[13]

The condition to confine fast electrons along the guide element is expressed as[8,14]

$$B_\phi L_\phi \geq \frac{P_f}{e}(1 - \cos\theta_d), \tag{2}$$

where B_ϕ is the azimuthal magnetic flux density, L_ϕ is the azimuthal magnetic field width, $P_f = \gamma_f v_f m_e$ is the fast electron momentum, (γ_f is the Lorentz factor, v_f is the fast electron velocity), and θ_d is the fast electron divergence angle. Equation (2) implies that the product of $B_\phi L_\phi$ needs to be larger than the fast electron momentum to reflect the fast electrons back towards the guide element axis. A laser intensity-wavelength product of 10^{19} W cm$^{-2}\mu$m^2 gives an electron energy of 1.8 MeV and momentum of $\approx 2 \times 10^{-22}$ kg m s^{-1}; taking the divergence angle $\theta_d = 30°$ requires a $B_\phi L_\phi$ of 10^{-3} Tm for collimation. Clearly, higher divergence angles and kinetic energy will require larger $B_\phi L_\phi$.[8,15]

In our previous work,[16] we extended the use of high resistivity guide-elements embedded in low-Z substrates (see Refs. 9, 10, and 12) to a graded-resistivity-interface target by using a range of different materials between the core and substrate to form a linear resistivity gradient at the interface. This resulted in a higher $B_\phi L_\phi$ and improved the fast electron beam collimation. Here, we take a similar approach, but use new Z profiles to form the resistive gradient and in this work structure the high-Z guide-element component of the target. The result is a $B_\phi L_\phi$ product that is similar to what was achieved in Refs. 9, 10, and 12, which sufficiently confines and collimates the fast electrons with the expectation that these new guides should be no better or worse than the earlier designs. Yet, what we find is improved heating-at-depth; we observe higher temperature tens of microns along the guide with a reduction in the temperature gradient. This results from a larger L_ϕ. There is less structure along the whole guide, albeit without ideal homogeneity of heating. The smoother heating structure results from a reduction in the magnetic fields inside the guide wire, which interferes with electron propagation ultimately driving electron beam filamentation.

[a)]Authors to whom correspondence should be addressed: reemyork@gmail.com raba500@york.ac.uk

The paper is structured as follows: Sec. II contains a description of resistive guide targets and hybrid particle-in-cell ZEPHYROS modeling approach. In Sec. III, we compare and discuss ZEPHYROS simulations of a simple guide embedded in a substrate with the three graded-resistivity-interface guides embedded in a substrate.

II. RESISTIVE GUIDE TARGET WITH RESISTIVITY GRADED CORE

Figure 1 shows 2-dimension z-x plane slices of the atomic number for (a) a step change between the high resistivity guide-element and low resistivity substrate, a simple resistive guide-element and (b) a graded resistivity change between the guide-element and substrate, where the grading is applied to the resistive guide-element. The slices are taken in the mid y-direction along the x-direction. The CH substrate in these targets (with density 1.0 g cm^{-3} and average atomic number Z = 3.5) has a square cross-section of length 50 μm in y- and z-directions and length 100 μm in the x-direction. The embedded wire is located in the middle of this substrate with a circular cross-section of diameter 10 μm and is co-linear along the length of CH substrate. In a simple resistive guide,[15] Fig. 1(a), the high resistivity guide-element is aluminium with density of 2.7 g cm^{-3} and atomic number 13. Figure 1(b) shows the graded resistive guide; the guide-element has a core of aluminium with density 2.7 g cm^{-3} and Z = 13 and then from the surface of the aluminium core, the atomic number linearly decreases to Z = 6, density 2.2 g cm^{-3} (carbon). The composition of the graded region of the guide-element in

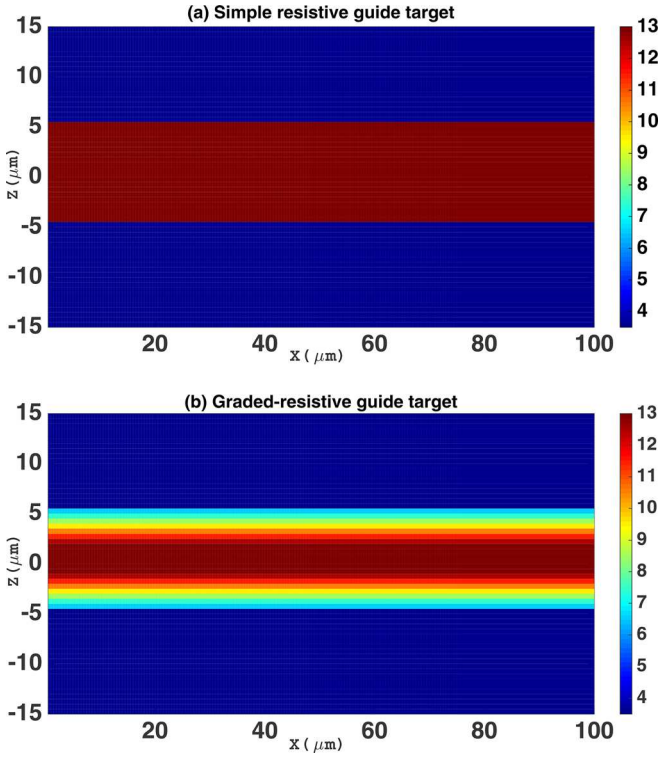

FIG. 1. Atomic number maps of (a) a simple resistive guide with an aluminium guide-element embedded in plastic and (b) a graded-resistive guide with a guide-element composed of an aluminum core clad in a sleeve of material of decreasing atomic number from Z = 13 to Z = 6 (carbon).

Fig. 1(b) is varied between the two different Z materials according to[8]

$$Z_{av} = Z_h\psi + Z_l(1-\psi), \tag{3}$$

$$n_i = n_h\psi + n_l(1-\psi), \tag{4}$$

where n_i is the ion density, h and l are denoted as a high-Z material and low-Z material, respectively, and ψ is a mixed fraction of materials h and l. The form used for ψ is

$$\psi = \begin{cases} h & \psi = 1 \\ l & \psi = 0 \\ \text{linear interpolation} & 0 < \psi < 1. \end{cases} \tag{5}$$

Figure 2 shows the radial atomic number profile for four different targets. The first, referred to as Target A, is shown in (a). This a simple resistive guide, with an aluminium wire embedded in a plastic substrate. Figures 2(b)–2(d) show three targets with a guide-element constructed of an aluminium core surrounded or sleeved in a layer of material of decreasing atomic number. The guide-elements in these targets are atomic number graded from Z = 6 at $z = \pm 5\,\mu$m to Z = 13, for Target B at $z = \pm 3.5\,\mu$m, Target C at $z = \pm 2.5\,\mu$m, and for Target D at $z = \pm 1.5\,\mu$m. This enables the testing of the guide-element with a different diameter of aluminum (high resistivity) core. The dashed lines in these figures show the diameter of aluminium core in each case.

Simulations were performed for these four targets using the three-dimensional particle-in-cell (PIC) hybrid code ZEPHYROS,[13] which is based on the hybrid method developed by Davies.[17,18] A 200 × 100 × 100 μm^3 grid was used with a 0.5 μm cell size in each direction. The number of macroparticles injected into each cell within the focal spot was 126. The laser irradiation intensity was 1.3×10^{20} W cm^{-2}. It is assumed that 30% of the laser energy couples to the fast electrons with the energy distribution of the fast electrons taken from the reduced Wilks' ponderomotive scaling.[19,20] The fast electron temperature is 2.7 MeV. A fast electron beam is injected into each target centered at (0,0,0), i.e., at the center of the aluminium core. The temporal profile of the fast electron beam is top-hat shaped with a pulse duration of 2 ps. The focal spot radius, r_{spot}, is 3.5 μm with intensity profile $\propto \exp[-\frac{r^2}{2r_{spot}^2}]$. The fast electron angular distribution is uniform over a divergence angle θ_d of 50°. The resistivity uses the Lee and More model[21] and a minimum mean free path of $5r_s$, where $r_s = (3/4\pi n_i)^{1/3}$ is the interatomic spacing and n_i is ion density. To prevent fast electron beam filamentation inside the guide and obtain uniform fast electron collimation, it is necessary to ensure that the laser radius spot, r_{spot}, is greater than the aluminium core radius, r_{core}, such that

$$\chi = \frac{r_{core}}{r_{spot}} < 1. \tag{6}$$

The aluminium core radius r_{core} and the ratio, χ, to the spot radius for Targets A to D are given in Table I.

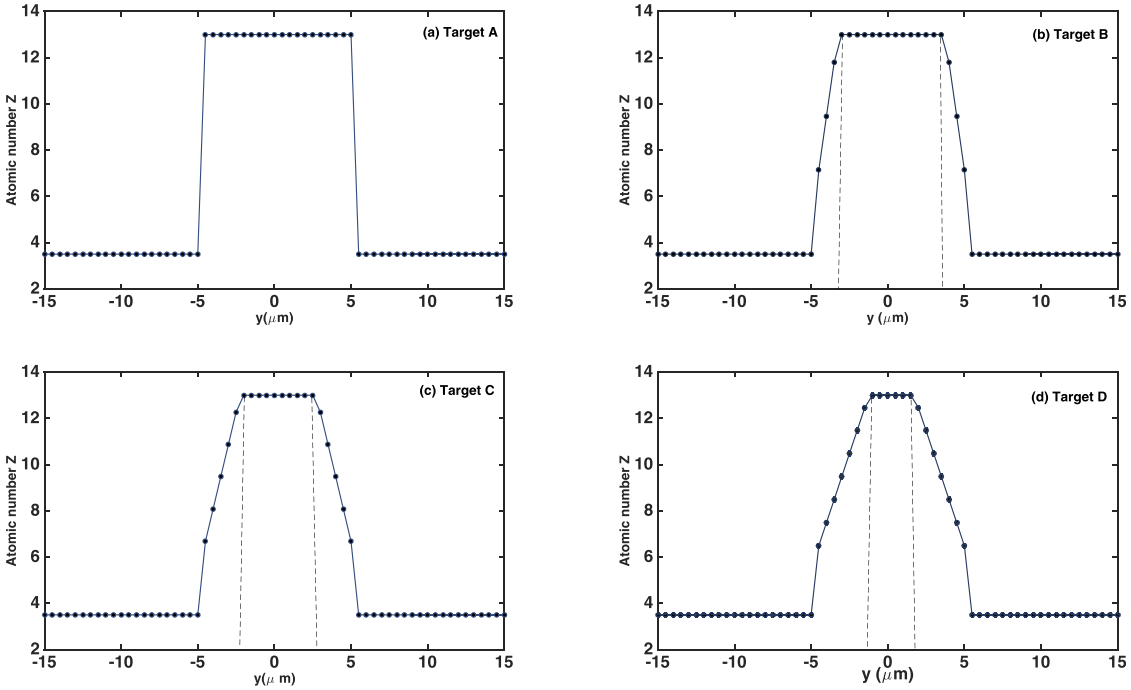

FIG. 2. Radial atomic number profile across the central of the targets. (a) shows a simple resistive guide with an aluminium guide-element embedded in plastic. (b), (c), and (d) show profiles for graded-resistive guide with decreasing atomic number at the edge of the aluminium core. The diameter of the aluminium core is indicated by the vertical dashed lines. The radius of this core, r_{core}, is 3.5 μm, 2.5 μm, and 1.5 μm respectively.

TABLE I. Table of radius of aluminium core, and ratio to spot radius, χ, for each Targets A to D.

Simulation	r_{core} (μm)	χ [Eq. (6)]
Target A	5	1.4
Target B	3.5	1
Target C	2.5	0.7
Target D	1.5	0.4

III. RESULTS

A. Effect of resistive grading on a collimating magnetic field

Figures 3(a)–3(d) show x-z images of the magnetic fields generated in Targets A to D at 2.2 ps after injecting the fast electrons. These images are taken at the mid-plane of y and in each case, an azimuthal magnetic field is generated at the interface between the guide-element and the substrate. This magnetic field is central to guiding and collimating of the fast electrons. Figures 3(a)–3(c) show magnetic fields that grow in the interior of the guide-elements; these interior

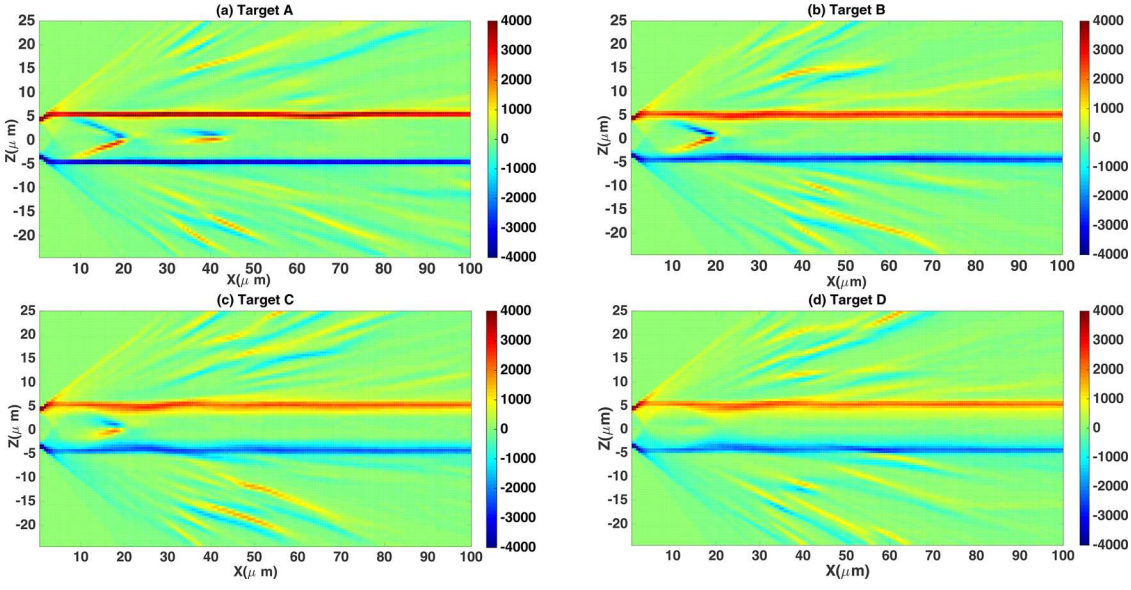

FIG. 3. Simulated magnetic field maps in Targets A–D (in Tesla) in the y midplane taken at 2.2 ps after the injection of the fast electron beam.

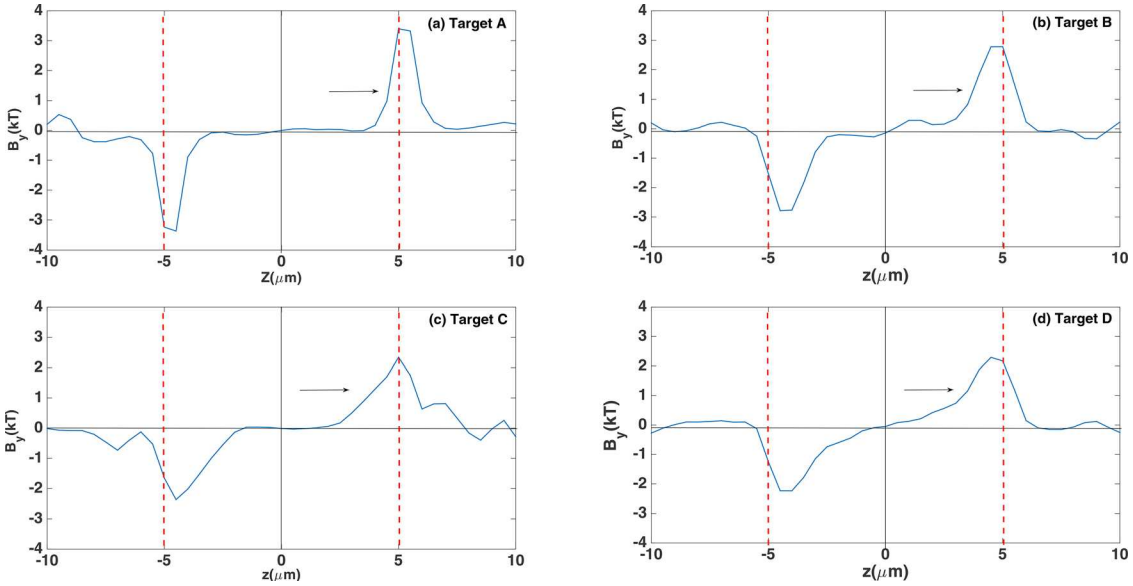

FIG. 4. Cross-sections of B_ϕ the magnetic field, as a function of z at $x = 10\,\mu$m for Targets A–D. These cross-sections are taken at 2.2 ps and are limited to $-10 < z < 10\,\mu$m in y midplane. The dashed lines show the boundaries of the guide-element. The arrow shows the gradient in the magnetic field inside the guide-element.

fields occur close to the substrate interface at approximately $x = 10\,\mu$m along the guide element and converge towards the central axis at approximately $x = 20\,\mu$m. Figure 3(a) shows a second interior field close to $x = 40\,\mu$m. The interior fields are most significant for Target A, the simple resistive guide. Interior magnetic fields are not observed in Fig. 3(d). The formation of "interior" magnetic fields is due to inhomogeneous propagation of the fast electrons. This results from the divergent flow of electrons[22] due to the gradient in the fast electron current density. The reduction and minimization of interior magnetic fields and electron beam filamentation are a key requirement for uniform guide-element heating. Graded resistivity guides limit the divergent of the fast electron beam.

Figure 4 shows the cross-sections of the azimuthal magnetic field B_ϕ taken at $x = 10\,\mu$m; this is close to the electron beam injection surface. Each cross-section is taken in the y midplane at 2.2 ps. The guide-element substrate interface is at $z = \pm 5\,\mu$m; as indicated by the vertical dashed lines, the azimuthal magnetic field peaks close to this boundary and extends into the substrate as well as the guide-element. The width of the collimating magnetic field, L_ϕ, differs from target to target. The measurement of L_ϕ extracted from Fig. 4 is listed in Table II. Target A has the smallest L_ϕ. For targets with graded-resistivity guide-element, the width of the collimating magnetic field increases. For example, L_ϕ, is $1.77\,\mu$m for Target B compared to $2.04\,\mu$m in Target D. The difference in L_ϕ is about 13%.

TABLE II. Table of the inferred L_ϕ, L_B, and $B_\phi L_\phi$ extracted from simulations shown in Fig. 4 (i.e., at 2.2 ps and $x = 10\,\mu$m in y midplane) of a simple resistive guide (Target A) and graded resistivity guides (Targets B to D) taken in each simulation.

Simulation	r_{core} (μm)	L_ϕ (μm)	L_B (μm)	$B_\phi L_\phi$ ($\times 10^{-3}$ Tm)
Target A	5	1.19	0.45	3.21
Target B	3.5	1.77	0.65	3.46
Target C	2.5	1.90	1.59	3.38
Target D	1.5	2.04	1.58	3.19

The magnetic field scale length, L_B, estimated from Fig. 4 using $L_B = (B_\phi/|dB_\phi/dz|)$, is listed in Table II. These values give some indication about the gradient in the magnetic field. For Target A, Fig. 4(a), the gradient in the magnetic field is steep and results in a region of significant magnetic field inside the guide element. In comparison, the magnetic field gradients in Targets B to D, Figs. 4(b)–4(d), are increasingly shallow and extended with the magnetic field in Target D permeating throughout the guide element. The inclusion of a resistivity gradient in the guide element increases L_B, which influences fast electron transport and improves the electron uniformity across and along the guide element. Furthermore, this improvement occurs for $B_\phi L_\phi$, which is similar in all targets (see Table II). The more complex targets do not increase $B_\phi L_\phi$ yet using these targets improves the electron beam uniformity and target heating. This results from increases in both L_ϕ and L_B, which suppress the growth of magnetics field interior to the guide element.

In a sharp resistivity change, for example, Target A, strong azimuthal magnetic fields with steep gradients form at the material interfaces resulting in a specular scattering of fast electrons as described in Ref. 22. Our analysis shows for targets with extended resistivity gradients (Targets B to D) in the high-Z guide; the azimuthal magnetic fields are extended and the gradients are reduced. The confinement of the fast electrons is enhanced by the extended magnetic field. With a sample particle pusher code, we find that the electron turns back toward the axis in Target A, for example, at $x = 3\,\mu$m while this occurs at $x = 1.5\,\mu$m in Target D. The simulations show that electrons oscillate in the guide with electrons in Target D traversing a shorter path. This limits the electron beam filamentation improving fast electron

current density uniformity, and whilst confining the electrons to a narrower region. This enables heating to higher temperatures deeper in the target.

B. Resistive guide heating

The resulting temperatures of the resistive guide (the substrate temperatures are not shown) are illustrated in Figs. 5(a)–5(d). These show x-z contour images of temperatures in eV in the y midplane at 2.2 ps. Target heating results from resistive scattering of the return current.[23] The temperature is highest, reaching 4 keV, close to the fast electrons injection site and fall to temperatures <1 keV close to the edge of the guide element and with distance along the length of the guide. In addition, for the simple resistive guide, Fig. 5(a), simulations show a significant structure on the temperature profile along the guide with low temperature (<1000 eV) regions on axis around $x = 15\,\mu$m and $40\,\mu$m. This results from filamentation in the return current due to the internal magnetic fields shown in Fig. 3(a). The temperature structure is reduced in the graded-resistivity-interface guide targets. An additional benefit of the improved fast electron confinement is a small temperature gradient along these guides between $x = 15\,\mu$m and $x = 100\,\mu$m. Target D, Fig. 5(d), which has the widest graded resistivity region, shows the least amount of temperatures structure and the smallest temperature gradient.

The Ohmic heating gives a background material heating rate that is proportional to the fast electron current density squared[24]

$$\frac{\partial T}{\partial t} = \frac{2}{3k_B n_e}\eta \vec{j}_f^{\,2}, \tag{7}$$

where k_B is the Boltzmann constant, n_e is the background electron density, η is the resistivity and $\vec{j}_f$ is the fast electron current density. In dense plasmas, the fast electron current is very nearly balanced by a cooler and more collisional return current;[23] as a result, the guide element heating is sensitive to the uniformity and collimation of the fast electrons across and along the guide element. In comparison to the simple guides, increased temperatures and lower gradients in the graded guides result from the confinement of electrons to a region of smaller radius. To understand this, we look at $\vec{j}_f^{\,2}$ in both targets A and D. In Fig. 6, we show $\vec{j}_f^{\,2}$ along the center of the simple (Target A) and graded guide (Target D) at the 2 ps. The fast electron density is highest in Target D (we note the decrease in the $\vec{j}_f^{\,2}$ in the region $7 \le z \le 15\,\mu$m) followed by a peak and then a drop. This explains the temperature difference between the targets A and D in Fig. 7, which is approximately 600 eV at $x = 50\,\mu$m where $\vec{j}_f^{\,2}$ differs by a factor of 2.

The total energy deposition using the thermal energy of electron per volume

$$U_e = \frac{3}{2} n_e e T, \tag{8}$$

$$E_e = \int_V U_e dV, \tag{9}$$

where e is the electron charge, is calculated. For the total radius of the wire (core plus the graded resistivity region), $r_{wire} = 5\,\mu$m, the energy deposition is comparable. However, Target D has core, $r_{core} = 1.5\,\mu$m much smaller than Target A. This, and the enhanced confinement of the electrons, results in a higher energy deposition at the center of the wire for Target D compared with Target A. The difference is a

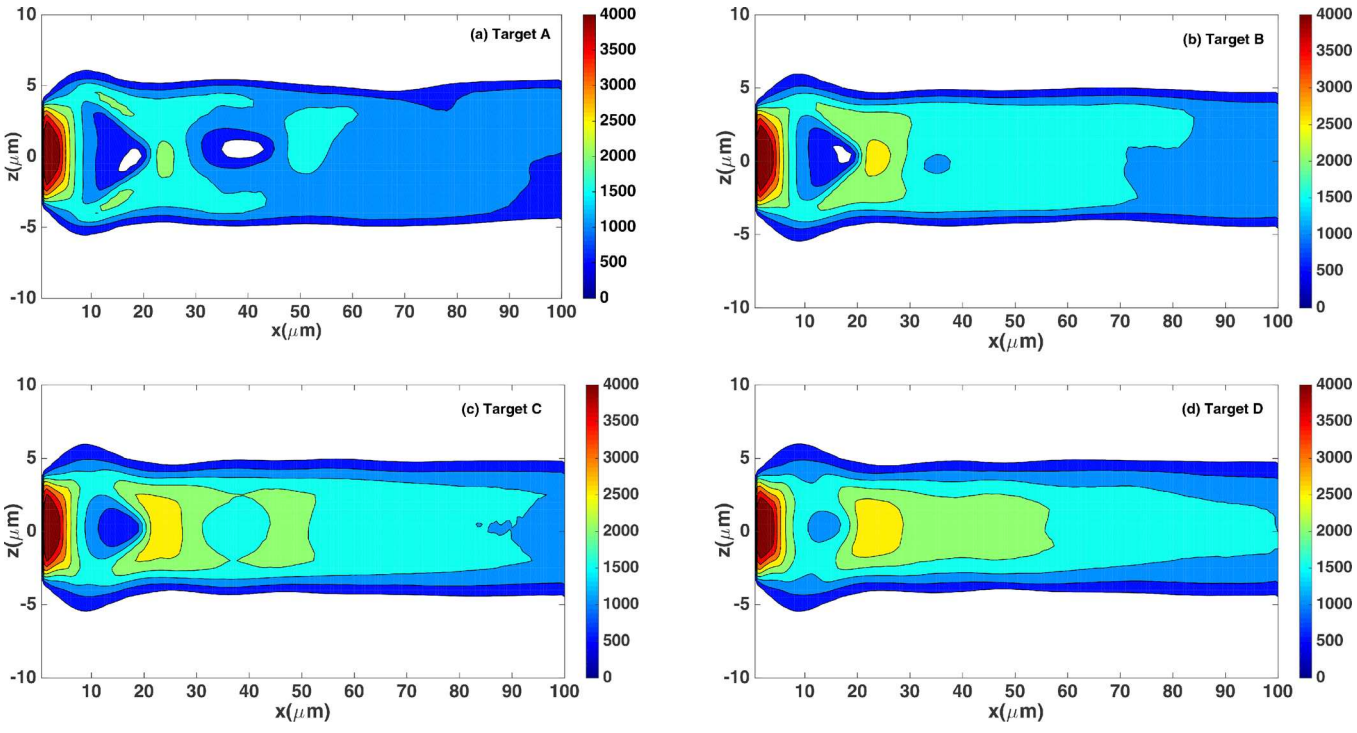

FIG. 5. Contour plots of the resistive guide temperature in eV at 2.2 ps for Targets A–D, respectively, along the x-direction in the y midplane.

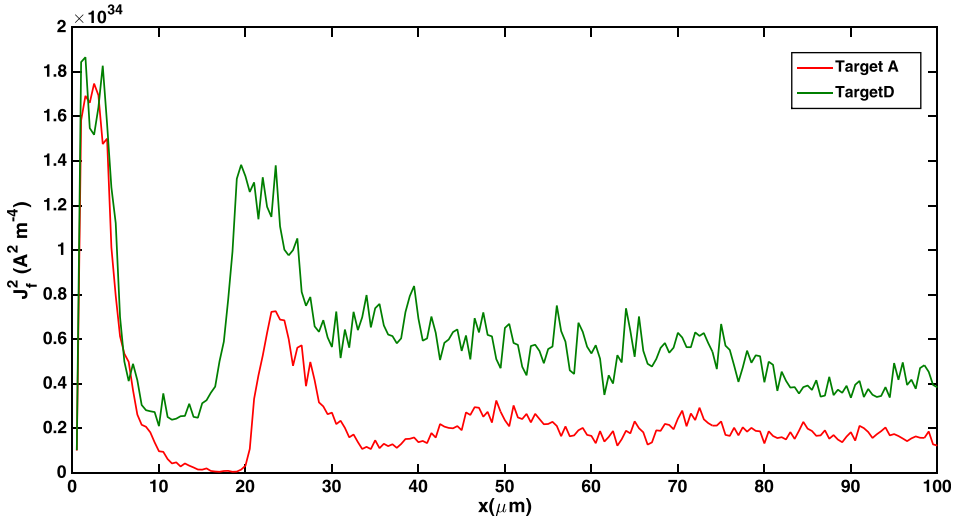

FIG. 6. Plots of the square fast electron current density in A^2m^{-4} at the end of the laser pulse 2 ps in Targets A and D.

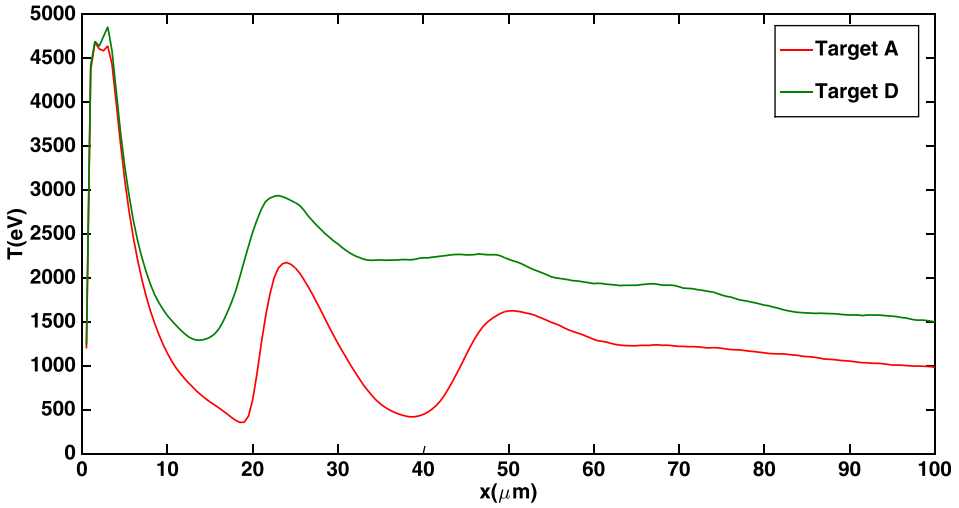

FIG. 7. Line-out of the background temperature in eV at 2.2 ps in Target A and D along the x-direction at the center of y and z.

factor of 1.5. This makes the central region of Target D higher temperature than Target A. This is in line with Fig. 7.

IV. CONCLUSION

We have described the improvement in the collimating magnetic field and resistive guide heating when using a graded-resistivity guide element in a resistive guide target. The principal result is $B_\phi L_\phi$ similar to what was observed before but with an extended magnetic field and shallower magnetic field gradient. By extending the magnetic field over much of the guide element, fast electrons will deflect over much of the guide, and these tend to smooth out any current density gradients eliminating interior magnetic field. In this situation, the fast electron transport is governed by an increasingly diffusive reflection in an extended magnetic field at the guide–substrate interface. As a result, fast electron confinement improves and an increased heating-at-depth occurs. We observe higher temperature tens of microns along the guide with a reduction in the temperature gradient. Furthermore, electron beam, and hence temperature, inhomogeneity is reduced by extending the length of the magnetic field and reducing the field gradient at the interface.

ACKNOWLEDGMENTS

The authors thank C. Spindloe from the Target Fabrication Group, CLF for helpful discussions on the manufacture of resistive guide targets and are grateful for the use of computing resources provided by STFC's Scientific Computing Department. The author (R.A.B.A.) was supported by a grant from the "Research Center of the Female Scientific and Medical Colleges," Deanship of Scientific Research, King Saud University. APLR is grateful for the support from the ERC via STRUCMAGFAST Grant (ERC-STG-2012).

[1]P. Gibbon, *Short Pulse Laser Interactions with Matter* (World Scientific Publishing Company, 2004).
[2]K. L. Lancaster, J. S. Green, D. S. Hey, K. U. Akli, J. R. Davies, R. J. Clarke, R. R. Freeman, H. Habara, M. H. Key, R. Kodama *et al.*, Phys. Rev. Lett. **98**, 125002 (2007).
[3]J. S. Green, V. M. Ovchinnikov, R. G. Evans, K. U. Akli, H. Azechi, F. N. Beg, C. Bellei, R. R. Freeman, H. Habara, R. Heathcote *et al.*, Phys. Rev. Lett. **100**, 015003 (2008).
[4]J. R. Davies, A. R. Bell, and M. Tatarakis, Phys. Rev. E **59**, 6032 (1999).
[5]A. R. Bell, J. R. Davies, and S. M. Guerin, Phys. Rev. E **58**, 2471 (1998).
[6]A. R. Bell and R. J. Kingham, Phys. Rev. Lett. **91**, 035003 (2003).
[7]L. Gremillet, G. Bonnaud, and F. Amiranoff, Phys. Plasmas **9**, 941 (2002).
[8]A. P. L. Robinson and M. Sherlock, Phys. Plasmas **14**, 083105 (2007).

[9]B. Ramakrishna, S. Kar, A. P. L. Robinson, D. J. Adams, K. Markey, M. N. Quinn, X. H. Yuan, P. McKenna, K. Lancaster, J. Green *et al.*, Phys. Rev. Lett. **105**, 135001 (2010).
[10]S. Kar, A. P. L. Robinson, D. C. Carroll, O. Lundh, K. Markey, P. McKenna, P. Norreys, and M. Zepf, Phys. Rev. Lett. **102**, 055001 (2009).
[11]A. P. L. Robinson, H. Schmitz, J. S. Green, C. P. Ridgers, and N. Booth, Plasma Phys. Controlled Fusion **57**, 064004 (2015).
[12]A. P. L. Robinson, H. Schmitz, J. S. Green, C. P. Ridgers, N. Booth, and J. Pasley, Phys. Plasmas **22**, 043118 (2015).
[13]A. P. L. Robinson, D. J. Strozzi, J. R. Davies, L. Gremillet, J. J. Honrubia, T. Johzaki, R. J. Kingham, M. Sherlock, and A. A. Solodov, Nucl. Fusion **54**, 054003 (2014).
[14]A. P. L. Robinson, M. Sherlock, and P. A. Norreys, Phys. Rev. Lett. **100**, 025002 (2008).
[15]A. P. L. Robinson, H. Schmitz, and J. Pasley, Phys. Plasmas **20**, 122701 (2013).
[16]R. A. B. Alraddadi, A. P. L. Robinson, N. C. Woolsey, and J. Pasley, Phys. Plasmas **23**, 072706 (2016).
[17]J. R. Davies, Phys. Rev. E **65**, 026407 (2002).
[18]J. R. Davies, A. R. Bell, M. G. Haines, and S. M. Guerin, Phys. Rev. E **56**, 7193 (1997).
[19]S. C. Wilks, W. L. Kruer, M. Tabak, and A. B. Langdon, Phys. Rev. Lett. **69**, 1383 (1992).
[20]M. Sherlock, Phys. Plasmas **16**, 103101 (2009).
[21]Y. T. Lee and R. M. More, Phys. Fluids **27**, 1273 (1984).
[22]A. P. L. Robinson and H. Schmitz, Phys. Plasmas **20**, 062704 (2013).
[23]A. R. Bell, J. R. Davies, S. Guerin, and H. Ruhl, Plasma Phys. Controlled Fusion **39**, 653 (1997).
[24]R. J. Garland, M. Borghesi, and A. P. L. Robinson, Phys. Plasmas **23**, 083116 (2016).